Magnetic force imaging of a chain of biogenic magnetite and Monte Carlo analysis of

tip–particle interaction

Magnetic force imaging of a chain of biogenic magnetite and Monte Carlo analysis of tip–particle interaction

André Körnig[1], **Markus A Hartmann**[2], **Christian Teichert**[2], **Peter Fratzl**[1] **and Damien Faivre**[1]

[1] Department of Biomaterials, Max Planck Institute of Colloids and Interfaces, Science Park Golm, 14424 Potsdam, Germany
[2] Institute of Physics, Montanuniversität Leoben, Franz-Josef Strasse 18, 8700 Leoben, Austria

E-mail: damien.faivre@mpikg.mpg.de

Abstract

Magnetotactic bacteria form chains of magnetite nanoparticles that serve the organism as navigation tools. The magnetic anisotropy of the superstructure makes the chain an ideal model to study the magnetic properties of such an organization. Magnetic force microscopy (MFM) is currently the technique of choice for the visualization of magnetic nanostructures, however it does not enable the quantitative measurement of magnetic properties, since the interactions between the MFM probe and the magnetic sample are complex and not yet fully understood. Here we present an MFM study of such a chain of biological magnetite nanoparticles. We combined experimental and theoretical (Monte Carlo simulation) analyses of the sample, and investigated the size and orientation of the magnetic moments of the single magnetic particles in the chain. MonteCarlo simulations were used to calculate the influence of the magnetic tip on the configuration of the sample. The advantage of this procedure is that analysis does not require any *a priori* knowledge of the properties of the sample. The magnetic properties of the tip and of the magnetosomes are indeed varied in the calculations until the phase profiles of the simulated MFM images achieve a best match with the experimental ones. We hope our results will open the doors towards a better quantification of MFM images, and possibly a better understanding of the biological process *in situ*.

(Some figures may appear in colour only in the online journal)

1. Introduction

Magnetosomes are magnetite crystals, embedded in an organic membrane, that are synthesized by magnetotactic bacteria [1]. The bacteria are ubiquitous in sediments of freshwater and marine aqueous environments [2]. The bacteria form chains of magnetosomes by a process regulated by a combination of physical and biological forces, while particles, when isolated from the cells, often form closed ring structures [3–8]. The magnetosome properties (dimension, morphology, magnetic properties), as well as the magnetosome chain pattern (single chain, multiple chains and their cellular distribution), are biologically controlled so the same strain of bacteria always forms magnetosomes with the same mature size and morphology, and have the same magnetosome arrangements [2]. Therefore, the magnetosome chains have advanced as a model system for magnetic nanostructures, because a variety of magnetic properties arise from the varying particle dimension and organization observed in different strains, and particularly in terms of magnetic anisotropy [9–11].

Atomic force microscopy (AFM) [12] is widely used in surface science to characterize the topography and the physical properties of a broad spectrum of inorganic and

J. Phys. D: Appl. Phys. **47** (2014) 235403

A Körnig *et al*

organic materials at the nanoscale level. Its variant, magnetic force microscopy (MFM) [12], in turn enables the visualization of magnetic structures even in complex materials [13]. Besides MFM, there are several other techniques which allow the simultaneous imaging and quantification of magnetic structures. Bose-Einstein condensates, as magnetic sensors, take advantage of the high sensitivity of cold atoms to changes in the magnetic field, and allow the measurement of magnetic fields down to 300 pT, but with a spatial resolution of only 3 μm [14]. Electron Holography allows imaging of samples at a high spatial resolution of 1 nm, but with the drawback of having to work with extremely small and thin samples under a high vacuum [15]. Optical methods have very recently achieved a spatial resolution of 400 nm and a magnetic sensitivity of 100 μT [16]. Thus, MFM appears to be the technique of choice since it has the potential to achieve both high spatial (20 nm) and high field sensitivity (1 μT) resolution. In addition, these excellent resolutions are coupled with the advantage of working under environmental conditions, which is particularly important for the study of biologically relevant processes. However, MFM functionality is reduced because the interaction between the MFM probe and the magnetic sample are complex and not yet fully understood.

The magnetic properties of magnetosomes and magnetosome assemblies have so far been analysed in different ways, e.g. first-order reversal curve (FORC) diagrams, ferromagnetic resonance (FMR) spectroscopy, coercivity analysis, and remanence measurements [17–23]. These results pointed towards superior magnetic properties of the biological materials, compared with those of the synthetic equivalents [24]. The magnetosomes have therefore been tested for numerous bio- and nano-technological applications [25, 26]. The first attempts to quantify the magnetic properties of nanoparticles in general, and of chains of nanoparticles in particular, were performed on simple model systems using MFM, e.g. on magnetosomes [27–29]. Proksch *et al* initiated the study of biogenic magnetite chains by MFM [27]. The magnetotactic bacterium studied was freeze-dried in order to ensure that the magnetite chain was close enough to the MFM tip for detection of any magnetic signal. Proksch *et al* assumed that the magnetic moments of all magnetosomes were oriented along the chain axis, and did not consider the effect of re-orientation of magnetic moments due to the particle–particle and particle–tip interactions [27]. More recently, Wei *et al* focused on the magnetization reversal of a two-particle assembly. The particles were studied both in the absence of, and while applying, an external magnetic field [28]. In contrast to the work of Proksch, they assumed independent magnetic moments of the individual magnetosomes, and showed that the dipolar magnetic interaction between neighboring particles is strong enough to at least partly keep the magnetization along the chain axis.

Here, we present an AFM/MFM study of isolated magnetosomes assembled in a chain. By a combination of experimental and theoretical (Monte Carlo simulation) analyses, we investigate the size and orientation of the magnetic moments of the single magnetic particles in the chain. The Monte Carlo simulations were used to quantify the influence of the magnetic tip on the magnetic configuration

of the sample during measurement. The analysis does not require any *a priori* knowledge of the properties of the sample. In the simulations, the magnetic properties of the tip and of the magnetosomes are varied until the phase profiles of the simulated MFM images best match the experimental ones. The geometric parameters needed are obtained by the topographic analysis done by the AFM simultaneously with the magnetic measurements obtained by MFM.

2. Experiment

2.1. Magnetosome sample preparation

Magnetosomes were isolated from the *Magnetospirillum gryphiswaldense* strain MSR-1 as described in [30]. The isolated magnetosomes were washed with MiliQ water. The magnetosomes were concentrated magnetically by placing a strong neodymium magnet, and physically by centrifuging at 6000*g* for 5 min, the supernatant was removed and the magnetosomes were washed with MiliQ water. Washed magnetosomes were pipetted onto freshly cleaved mica which was placed between two magnets in order to get aligned magnetosome chains.

2.2. Atomic force microscopy

Atomic and MFM images were recorded using the commercially available nanowizzard III (JPK instruments, Berlin, Germany). For MFM experiments, silicon cantilevers with a hard magnetic, medium momentum cobalt alloy coating on the tip (MagneticMulti75-G, NanoAndMore, Wetzlar, Germany) were used. The thickness of the coating of the tip is ca. 50 nm and the tip radius is less than 60 nm. Prior to the measurements, the magnetization of the tip was saturated using a strong magnet. The topographical images were obtained in alternating current (ac) mode. MFM images were obtained in the hover mode, i.e. on the first scan, the cantilever directly scans the surface of the sample, and on the second scan (hover mode retrace), the cantilever is raised to a user-defined height, and follows the topographical pattern from the previous trace. On the first trace, short range interactions (i.e. Van der Waals forces) have the most significant effect and the topography is imaged. On the hover mode retrace, long range interactions such as magnetic forces are most prevalent, and the MFM image will therefore reflect the magnetic properties of the sample. These lift heights were in the range of 30–100 nm.

Evaluation of the cantilevers' spring constant k, and the quality factor Q, was performed with the internal software of the JPK nanowizzard, applying the thermal method [31]. The obtained values were $Q = 230$ ($\pm 10\%$) N m^{-1} and $k = 6.7$ ($\pm 5\%$) N m^{-1}, respectively.

The AFM and MFM images were analysed with the open source program Gwyddion [32]. The images were typically flattened and leveled by the three-point plane method to obtain the zero height and phase in the plane level. 3D images were generated using the same program. Profiles were exported from Gwyddion and analysed with Origin and Python.

2.3. Monte Carlo simulations

Monte Carlo simulations were performed to understand the phase contrast images obtained by the MFM measurements. All magnetic objects were treated as point dipoles, having a dipole moment $\boldsymbol{m}$. The magnitude of the dipole moments was kept constant during the simulations, while the direction of the moments of the magnetosomes was variable. For the calculation of the energy, only magnetic interactions were considered. The potential energy of a dipole moment $\boldsymbol{m}$ in a magnetic field $\boldsymbol{B}$ is defined as:

$$E = -\boldsymbol{m} \cdot \boldsymbol{B}$$

The magnetic field produced by a magnetic dipole at position $\boldsymbol{r}$ is given by:

$$\boldsymbol{B}(\boldsymbol{r}) = \frac{\mu_0}{4\pi} \left(\frac{3(\boldsymbol{m} \cdot \boldsymbol{r})\,\boldsymbol{r}}{r^5} - \frac{\boldsymbol{m}}{r^3} \right)$$

where μ_0 is the vacuum permeability. Consequently, the energy of N magnetosomes is given by:

$$\begin{aligned}
E_{\text{chain}} &= -\sum_{i,j>i}^{N} \boldsymbol{m}_i \cdot \boldsymbol{B}_j \\
&= -\frac{\mu_0}{4\pi} \sum_{i,j>j}^{N} \left(\frac{3(\boldsymbol{m}_i \cdot \boldsymbol{r}_{ij})(\boldsymbol{m}_j \cdot \boldsymbol{r}_{ij})}{r_{ij}^5} - \frac{m_i m_j}{r_{ij}^3} \right)
\end{aligned}$$

where m_i and m_j are the magnetic moments and r_{ij} is the connecting vector between the two magnetosomes i and j. The energy between the magnetosomes and the tip is:

$$\begin{aligned}
E_{\text{tip-chain}} &= -\sum_{i}^{N} \boldsymbol{m}_i \boldsymbol{B}_{\text{tip}} \\
&= -\frac{\mu_0}{4\pi} \sum_{i}^{N} \left(\frac{3(\boldsymbol{m}_i \cdot \boldsymbol{r}_i)(\boldsymbol{m}_{\text{tip}} \cdot \boldsymbol{r}_i)}{r_i^5} - \frac{m_i m_{\text{tip}}}{r_i^3} \right)
\end{aligned}$$

where r_i is the connecting vector between magnetosome i and the tip, and m_{tip} is the magnetic dipole moment of the tip. The total energy of the system is the sum of these two contributions.

During the simulation, the positions of the magnetosomes and the trace of the tip were defined. One simulation step consisted of choosing one magnetosome randomly and changing the direction of its dipole moment from m_i^{old} to m_i^{new}. Then the energy difference $\Delta E = E_{\text{new}} - E_{\text{old}}$ was calculated according to the former equations. Following the Metropolis algorithm [33] the new dipole moment was accepted with a probability:

$$p = \min \left(1, e^{-\frac{\Delta E}{k_{\text{B}} T}} \right)$$

where the temperature T was set to room temperature and k_{B} is the Boltzmann constant.

2.3.1. Calculation of the phase shift.
The oscillating MFM cantilever is sensitive to force gradients, since these lead to a change of the effective spring constant: $k_{\text{eff}} = k - F_z'$ [34].

If the cantilever is driven at its resonant frequency, small force gradients $F_z' \ll k$ lead to phase shifts of

$$\Delta \Phi = -\frac{Q}{k} \frac{\partial}{\partial z} F_z,$$

where k is the spring constant and Q is the quality factor of the MFM cantilever, which were obtained experimentally [35].

Prior to the measurements, the tip was magnetically saturated by a strong magnet with its dipole moment pointing into the negative z-direction. Because the magnetic moment of the tip is usually considerably larger than the magnetic moments of the magnetosomes, we assume a constant value of $m_{\text{tip}} = -m_{\text{tip}} e_z$.

As $F = -\nabla E = \nabla(\boldsymbol{m} \cdot \boldsymbol{B})$, the z component of the force is given by:

$$F_z = \frac{\partial}{\partial z} m_{\text{tip}} B_{\text{sample}}(\boldsymbol{r}) = -m_{\text{tip}} \frac{\partial}{\partial z} B_{\text{sample}}^z(\boldsymbol{r})$$

and results in a phase shift of:

$$\Delta \Phi = \frac{Q}{k} m_{\text{tip}} \frac{\partial^2}{\partial z^2} \sum_{i}^{N} B_z^i(\boldsymbol{r}_i) = \frac{Q}{k} m_{\text{tip}} \sum_{i}^{N} \frac{\partial^2}{\partial z^2} B_z^i(\boldsymbol{r}_i)$$

where $B_z^i(\boldsymbol{r}_i)$ is the z component of the magnetic field at the position of the tip, produced by the dipole moment of magnetosome i, connected to the tip position via vector r_i.

The dipole moment of one of the magnetosomes (the index i is neglected for clarity) at the position (P_x, P_y, P_z) is described by the vector components (m_x, m_y, m_z). The z component of the magnetic field $B(r) = \mu_0/4\pi((3(m \cdot r)r/r^5) - (m/r^3))$ at the position of the tip (x, y, z) is given by:

$$B_z(x, y, z) = \frac{\mu_0}{4\pi}$$
$$\times \left(\frac{3(m_x[x-P_x] + m_y[y-P_y] + m_z[z-P_z]) \cdot [z-P_z]}{\left([x-P_x]^2 + [y-P_y]^2 + [z-P_z]^2\right)^{\frac{5}{2}}} \right.$$
$$\left. - \frac{m_z}{\left([x-P_x]^2 + [y-P_y]^2 + [z-P_z]^2\right)^{\frac{3}{2}}} \right)$$

The second partial derivative of this expression with respect to z was solved analytically with the help of Mathematica (Wolfram, 2010).

For every position of the tip, three runs with 10^4 iterations over the rotation of the dipole moment of individual spins were performed. Whether the system had attained its equilibrium state was verified by monitoring the energy and checking its convergence to a constant mean value. At one tip position, the phase was calculated for each of the three runs, and the mean value was taken as the phase signal. The tip was then moved to the next position. The final dipole configuration of the last run was used as the starting configuration for the new position.

3. Results and discussion

Magnetosomes isolated from *Magnetospirillum gryphiswaldense* MSR-1 were studied [36]. Isolation of the
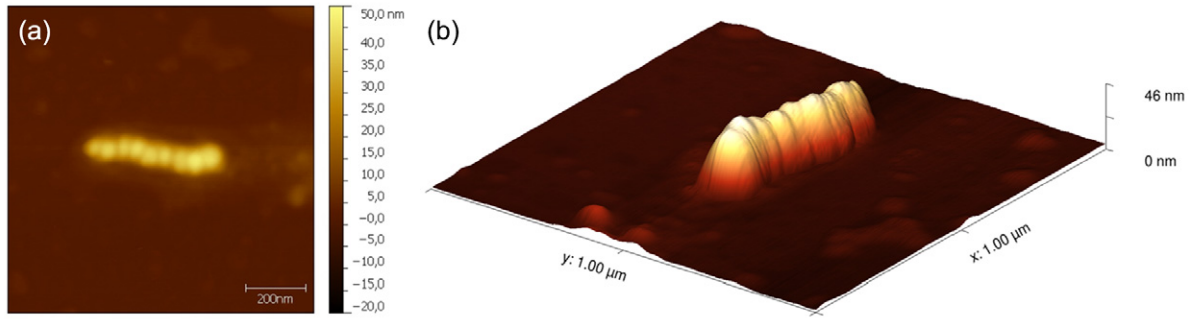
Figure 1. Topography of a chain of isolated magnetosomes obtained with an AFM tip (*a*). 3 D image of the same chain (*b*).

magnetosomes was performed following a published protocol [37] (see section 2). Figure 1 shows a topographic image of the sample obtained by a standard AFM scan, where nine magnetosomes can be seen, arranged in a rather straight line. The measured magnetosome height is 39.9 ($\pm$3.0) nm ($n = 9$). The edge-to-edge distance between two consecutive particles is found to be 48.9 ($\pm$4.8) nm. For isotropic particles like the magnetosomes, it is expected that height and distance have the same value. The observed difference arises most probably from the magnetosome membrane, since the magnetosomes are arranged on the substrate with intact membranes with a thickness of $\approx$4 nm [38]. The reduced height can be related to the shrinking of the magnetosome membrane during the drying process. The diameter for magnetosome magnetite particles from MSR-1 is typically 40 nm [1]. Thus, considering the thickness of the membrane, the observed average sizes are in good agreement with literature values.

The chain is then measured with a magnetically coated tip (from right to left in our case) (figure 2). In MFM measurements, which are recorded in the two-step hover mode (see section 2.2), each topography scan line is re-scanned with a user-defined distance between the tip and the sample (lift height). In this case, magnetic forces are dominant and can be quantified by the phase shift of the cantilever oscillation. Phase images of the scans obtained at different lift heights are shown in figure 2(*a*)–(*c*). The chain axis is also indicated in the figure, together with the corresponding one-dimensional phase profile along the axis and the previously obtained height profile (figure 2(*d*)–(*f*)). The detected phase shifts change dramatically with increasing lift height. The measured phase shift is negative, indicating an attractive force between tip and sample. Furthermore, the absolute value of the detected phase shift decreases with increasing lift height (from about $-0.6°$ at 30 nm to about $-0.2°$ at 100 nm). This is expected, since the magnetic field of the magnetosomes decays with the distance to the power of 3.

More interestingly, the shape of the profiles also change with different lift heights. These different shapes are determined by the interaction between the tip and sample. Depending on the interaction strength, i.e. the lift height, the magnetic interaction may change the orientation of the magnetic moment of the magnetosome. Qualitatively, at a 30 nm lift height when the tip is approaching the magnetosomes, the phase shift first decreases, indicating an attractive interaction, and then oscillates (figure 2(*d*)). When

the lift height is increased to 50 nm, this oscillation becomes extremely small, eventually vanishing in the noise level (left end of chain in figure 2(*e*)). However, the signal is not constant along the chain axis. Small bumps can be seen towards both ends of the chain (around positions of 350 nm and 600 nm, respectively). The shape of the signal obtained at the 100 nm lift height is very different than that obtained at lower lift heights (figure 2(*f*)). The phase profile takes a minimum close to the starting point of the scan at a position of $\sim$600 nm and increases towards the other end of the chain, even taking slightly positive values, which indicates repulsion between sample and tip.

Monte Carlo simulations have been performed to gain a better understanding of the interaction between the MFM tip and the individual magnetic moments of the magnetosomes in the chain. This interaction indeed determines the different shapes of the phase profiles we measured experimentally. Monte Carlo simulations allow detection of the equilibrium state of a system at a given temperature (here ambient temperature) by minimizing its free energy [33] (see section 2). The field of the tip is described as a magnetic dipole, with its magnetic moment pointing in the negative z-direction (the (positive) z-direction is assumed to be perpendicular to the plane of the magnetosomes directed to the tip). All the magnetosomes are assumed to have the same (geometric) size, and the size of their dipole moment, $m = M_s V$, is typically calculated using either the saturation magnetization of magnetite ($M_s = 480$ kA m^{-1}) or the oxidized version of the iron oxide, namely maghemite, ($M_s = 380$ kA m^{-1}) [39] to test for the nature of the particles. The volume of the magnetosomes is given by a sphere of radius $r_{Ms} = 20$ nm (see section 2). The distance between two magnetosome dipoles is set to $d = 50$ nm, and this is consistent with the topographical information. The value of the magnetic moment of the tip is given by the manufacturer as $m_{tip} = 10^{-16}$ A m^2.

In the simulations, he tip position is virtually moved at a constant lift height above the magnetosomes dipoles. This is a slight difference from the experiment, in which the tip position is adjusted to take the topography into account and keeps a constant height above the magnetosomes, with slight drops between the particles. Thus, in the simulations the distance between tip and sample is a bit larger than in the experiment, which reduces the effect of the non-uniform size of the magnetosomes. For every tip position, the average phase signal of the final configuration is determined.
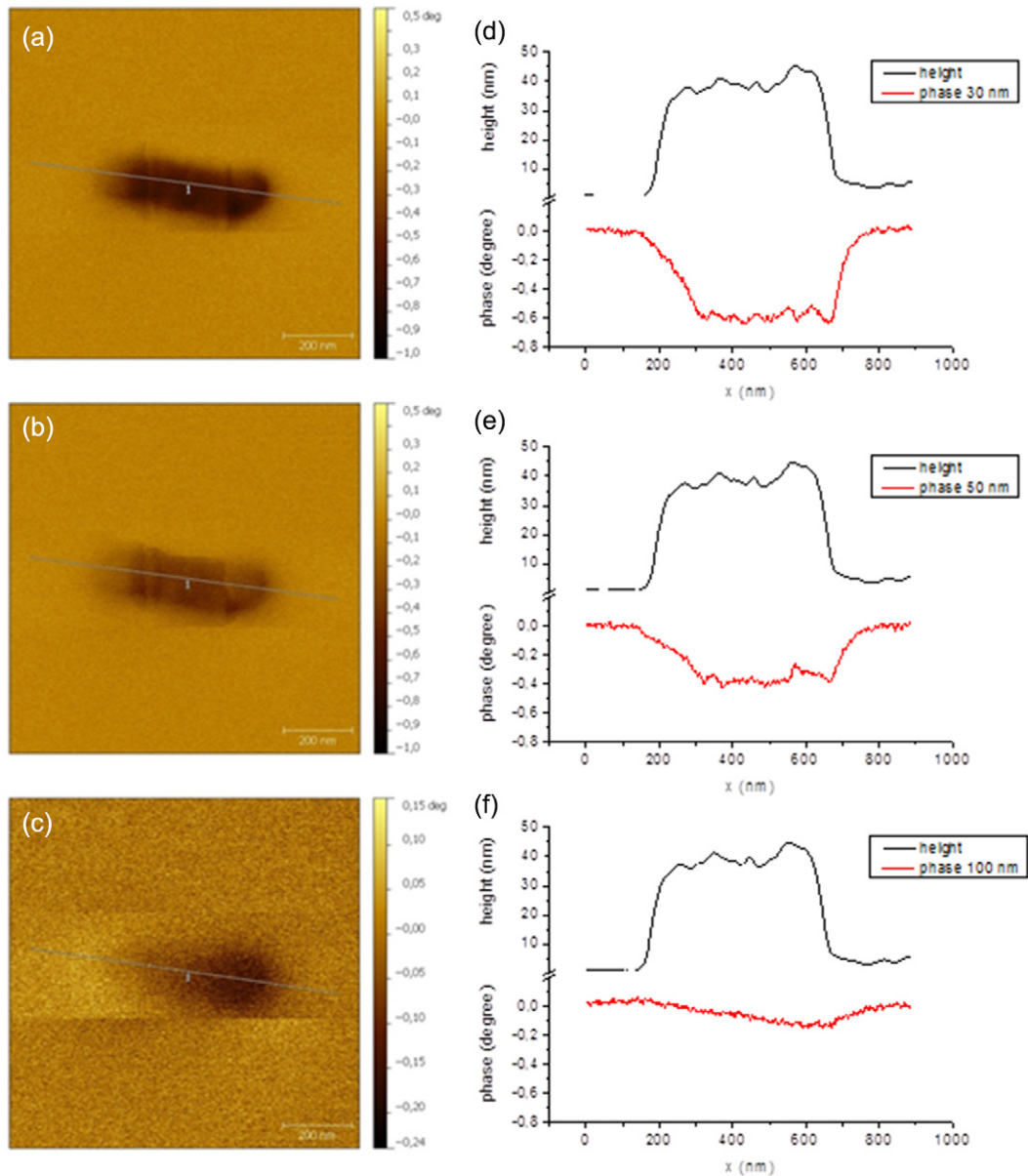
Figure 2. (*a*)–(*c*) Phase images of the chain of nine magnetosomes scanned from right to left and obtained at different lift heights: 30 nm (*a*), 50 nm (*b*) and 100 nm (*c*), respectively. (*d*)–(*f*) The phase profiles along the axis of the chain, as indicated by the straight lines in (*a*–*c*), are shown in red. The corresponding AFM height profiles are shown in black.

We varied the moment of the tip as well as the moment of the magnetosomes in the simulations in order to find out the parameters that best match our experimental results (see online Supplementary table S1 (stacks.iop.org/ JPhysD/47/235403/mmedia)). The main characteristic of a good match between experiment and simulation is (next to the phase shift values) the shape of the phase profiles at different heights. Typically, the shape of these phase profiles at all three heights can only be reproduced for a given set of parameters. The best fit was obtained for a value of 10^{-16} A m^2 for the magnetic moment of the tip, corresponding to the value provided by the probe manufacturer, and a value of 1.6×10^{-17} A m^2 for the magnetic moment of the single magnetosomes corresponding to magnetite, in agreement with values from literature [1]. This is indeed the only set of

parameters that enables the qualitative match of the profiles at all three lift heights. Figure 3 shows a comparison of simulated and measured phase profiles along the chain axis for the set of parameters explained above.

Despite the simplifications used in the theoretical analysis, e.g. the assumption of uniform magnetosome size, and the point dipole approximation, the phase profiles obtained from the simulations qualitatively match the experimentally obtained ones. The characteristic shapes of the profiles are reproduced: first, oscillations at low lift heights (figures 3(*a*) and (*d*)), second, jumps at medium lift heights (figures 3(*b*) and (*e*)) and, third, the constant decrease of the signal at large lift heights (figures 3(*c*) and (*f*)). A quantitative satisfactory match is only obtained for intermediate lift heights (figures 3(*b*) and (*e*)), while for small (figures 3(*a*) and (*d*)) and large
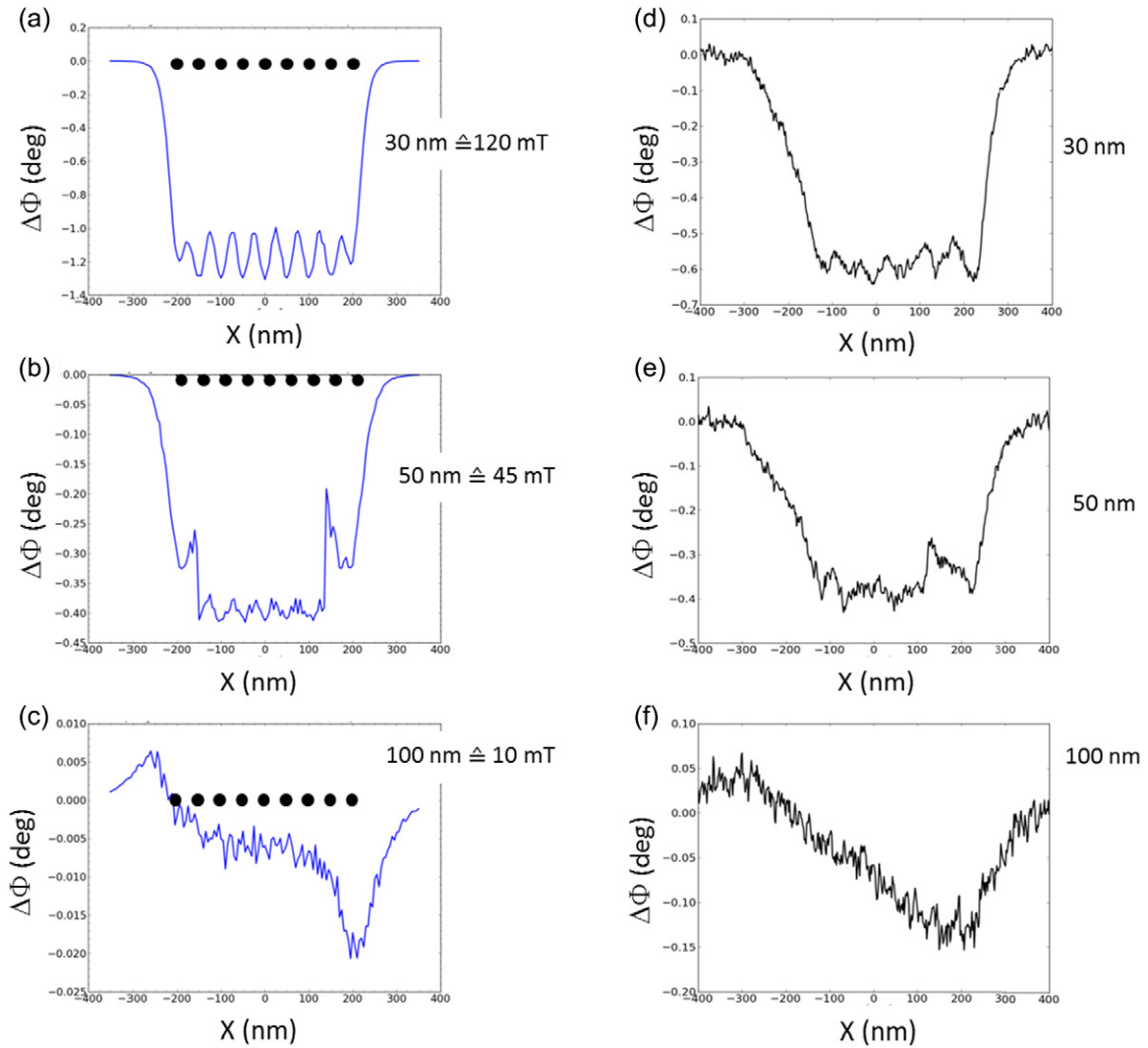
Figure 3. Comparison of simulated (*a*)–(*c*) and measured (from right to left) (*d*)–(*f*) phase profiles. The simulated phase signal is obtained by numerically analyzing equilibrium configurations of the magnetic moments obtained by Monte Carlo simulations for different lift heights as indicated on the graphs. The corresponding magnetic field of the tip in the plane of the magnetosome is also given. The size of the magnetic moment of the magnetosomes is 1.61×10^{-17} A m^2, corresponding to the saturation magnetization of magnetite $M_s = 480$ kA m^{-1}. The black dots at zero phase shifts indicate the positions of the nine magnetosomes. The experimental phase signals of MFM measurements are the same as those shown in figure 2, but are rescaled.

(figures 3(*c*) and (*f*)) lift heights, the absolute values of simulated and experimental phase shifts do not coincide. The experimentally obtained maximum of the phase shifts is twice that of the simulated one at 30 nm, and only a tenth at 100 nm lift height. These differences might arise from an effective screening of the magnetic fields due to the finite size of the magnetosomes and of the tip, which would be distance-dependent. Alternatively, it could be the consequence of contamination of the tip for some measurements, which in fact enlarges the probe to magnetosome distance. However, this disagreement between simulation and experiment is most probably due to the point dipole approximation that was used in describing the magnetic tip. In Häberle *et al* [40], it was shown that close to the tip the magnetic field decays with $1/r$ instead of with the $1/r^3$ dependence of a classical dipole. Thus, in the simulations the magnetic field effectively decays too fast, explaining why the simulations underestimate the

tip–magnetosome interaction with increasing distance. Most probably the agreement between simulation and experiment can be significantly improved by introducing a lift height dependent calibration factor, as proposed by Sievers *et al* in order to realize quantitative MFM measurements [41].

Interestingly, the simulations also reveal the influence of the magnetic moment of the tip on the orientation of the moments of the individual magnetosomes. At low lift heights, the influence of the tip is large, as expected (figure 4). In the absence of the magnetic field of the tip, the energetic ground state of the system is given by all magnetic moments of the magnetosomes, aligned along the chain. When the tip is directly above one magnetosome, its magnetic field is strong enough to re-orient the magnetic moment of the magnetosome. The magnetic moment then aligns with the field in the negative *z*-direction, leading to a strong field gradient at the tip and therefore to a big phase shift signal (figure 4(*b*)). When the
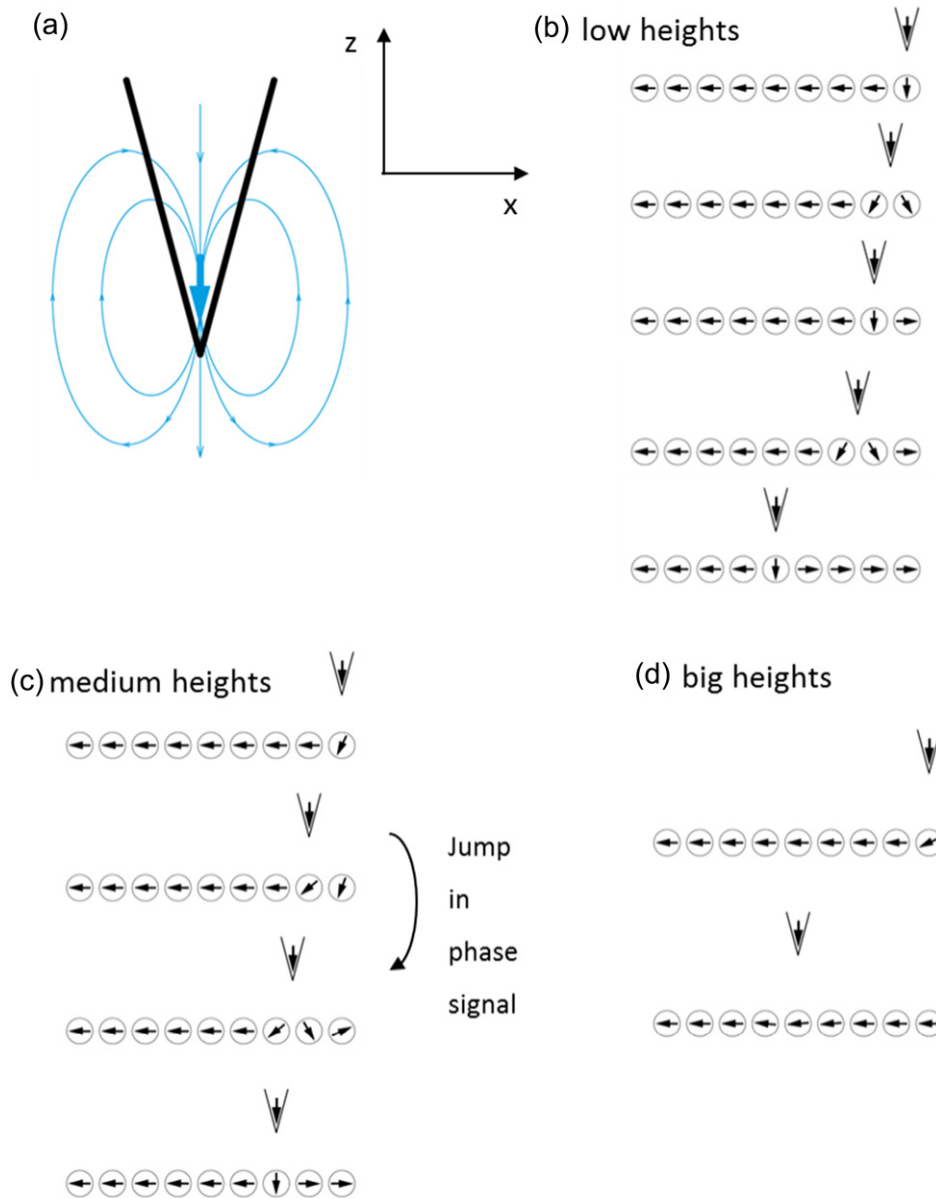
Figure 4. (*a*) The magnetic field of a point dipole with its magnetic moment aligned in the negative *z*-direction. A sketch of the tip influence on the magnetosome's dipole configuration is then presented (*b*)–(*d*). (*b*) Influence of the tip on the direction of the magnetic moments of the magnetosomes for low lift heights (30 nm). For medium lift heights (50 nm, (*c*) a jump occurs between positions 2 and 3); for big lift heights (100 nm, (*d*) only a little influence of the tip is observed (see text for full description of the interactions at the respective lift heights).

tip is above the gap between two magnetosomes, the field is still large enough for the moments of the magnetosomes to align with the—now tilted—field (figure 4(*b*)). Because the magnetic moment is now not fully oriented in the *z*-direction, the phase shift signal is smaller than in the case when the tip is directly above the magnetosome. This effect leads to the observed oscillations. When the tip is moved across the magnetosome, its magnetic moment re-aligns with the field of the tip, so it now essentially points in the *x*-direction, meaning an effective flip of the moment compared to the starting configuration. Therefore, a symmetric configuration would typically be expected when the tip scans from the other direction, even if the chain is oriented the same way, because the same types of interactions are obtained.

The jumps of the signal at medium lift heights (50 nm) are qualitatively explained by the competing influences of the magnetic moment of the tip and the moments of the other magnetosomes on any single particle (figure 4(*c*)). In contrast to the lower lift heights, the magnetosomes at the end do not completely align in the *z*-direction when the tip is directly above. The field of the other particles is strong enough to partly hold it back, and the moment only gets tilted. In particular, the field of the tip is not strong enough to directly flip the moment of the magnetosome when the tip passes the particle. It is only after the tip also passed the second magnetosome that the combined field is strong enough to flip the moments, resulting in a jump in the phase signal. For each following magnetosome, the adjacent dipole moments point in opposite

J. Phys. D: Appl. Phys. **47** (2014) 235403

A Körnig *et al*

directions, therefore there is no competition with the tip, and the dipole moments align with the tip.

At large lift heights (100 nm), the influence of the magnetic field of the tip on the orientation of the magnetosome dipoles is small (figure 4(*d*)). The magnetic moments of the other magnetosomes in the chain stabilize the dipole direction and prevent its alignment with the tip dipole. Thus, after the tip has passed all magnetosomes, the magnetic moments of these are anti-parallel to the field of the tip, resulting in the observed positive phase shift, indicating repulsive forces.

The combination of MFM measurements and Monte Carlo simulations permits a much deeper understanding of the magnetosome—MFM tip interaction in a chain of particles than has been previously reported. Proksch *et al* quantified the magnetic moment of the chain without any description of the interaction between the magnetosomes and the tip [27]. Furthermore, their approach cannot easily be used for systems for which no *a priori* magnetic information is available. In fact, in the present approach no *a priori* information is needed.

Wei *et al* in turn proposed a more comprehensive description of the tip–magnetosome interaction, showing that isolated particles would easily be polarized by the MFM tip, whereas the orientation of the magnetic moments of magnetosomes in a chain would be stabilized by dipolar interactions among the particles [28]. However, the authors did not present any description of the phase profiles, certainly not at different lift heights.

4. Conclusions

We have experimentally studied a single chain of magnetic particles by MFM, and theoretically simulated the associated phase shift profiles by the use of Monte Carlo simulations. Despite the inevitable approximations made to make the problem theoretically tractable (e.g. describing the magnetic field of tip and magnetosomes as point dipoles), the simulated data fits well with the phase profiles that were observed experimentally. The simulations are rapid and enable the most comprehensive description of the interaction between an MFM tip with the magnetosomes in a chain. In particular, our model involves inter-particle interactions that were previously ignored, and thereby gives insights into the magnetic configuration of the single magnetic moments in the chain. The model clearly shows a more pronounced interaction of the tip with particles at the end of the chain as expected, and as experimentally observed. This is explained by the lower number of stabilizing neighbors of the particles close to the chain ends. The best correlation between experiments and simulations was obtained for a magnetic moment of the magnetosomes in the chain of about $1.6 \times 10^{-17}\,\mathrm{A\,m^2}$, corresponding to magnetite.

Acknowledgments

References

[1] Faivre D and Schüler D 2008 Magnetotactic bacteria and magnetosomes *Chem. Rev.* **108** 4875–98

[2] Lefèvre C T and Bazylinski D A 2013 Ecology, diversity, and evolution of magnetotactic bacteria *Microbiol. Mol. Biol. Rev.* **77** 497–526

[3] Faivre D *et al* 2010 The development of cellular magnetic dipoles *Biophys. J.* **99** 1268–73

[4] Klumpp S and Faivre D 2012 Interplay of magnetic interactions and active movements in the formation of magnetosome chains *Plos One* **7** e33562

[5] Komeili A *et al* 2006 Magnetosomes are cell membrane invaginations organized by the actin-like protein MamK *Science* **311** 242–5

[6] Scheffel A *et al* 2006 An acidic protein aligns magnetosomes along a filamentous structure in magnetotactic bacteria *Nature* **440** 110–5

[7] Philipse A P and Maas D 2002 Magnetic colloids from magnetotactic bacteria: chain formation and colloidal stability *Langmuir* **18** 9977–84

[8] Carillo M A, Bennet M and Faivre D 2013 The interaction of proteins associated to the magnetosome assembly in magnetotactic bacteria as revealed by two-hybrid two-photon excitation fluorescence lifetime imaging microscopy förster resonance energy transfer *J. Phys. Chem.* B **117** 14642–8

[9] Muxworthy A R and Williams W 2006 Critical single-domain/multidomain grain sizes in noninteracting and interacting elongated magnetite particles: implications for magnetosomes *J. Geophys. Res.* **111** B12S12

[10] Muxworthy A R and Williams W 2009 Critical superparamagnetic/single-domain grain sizes in interacting magnetite particles: implications for magnetosome crystals *J. R. Soc. Interface* **6** 1207–12

[11] Kasama T *et al* 2006 Magnetic properties, microstructure, composition, and morphology of greigite nanocrystals in magnetotactic bacteria from electron holography and tomography *Am. Mineral.* **91** 1216–29

[12] Meyer E, Hug H J and Bennewitz R 2004 *Scanning Probe Microscopy: The Lab on a Tip* (Berlin: Springer) p 210

[13] Yue L and Liou S 2011 Magnetic force microscopy studies of magnetic features and nanostructures *Scanning Probe Microscopy in Nanoscience and Nanotechnology 2* ed B Bhushan (Berlin: Springer) pp 287–319

[14] Wildermuth S *et al* 2005 Bose–Einstein condensates microscopic magnetic-field imaging *Nature* **435** 440

[15] Dunin-Borkowski R E *et al* 1998 Magnetic microstructure of magnetotactic bacteria by electron holography *Science* **282** 1868–70

[16] Le Sage D *et al* 2013 Optical magnetic imaging of living cells *Nature* **496** 486–9

[17] Moskovitz B M, Frankel R B and Bazylinski D A 1993 Rock magnetic criteria for the detection of biogenic magnetite *Earth Planet. Sci. Lett.* **120** 283–300

[18] Moskowitz B M *et al* 1989 A comparison of magnetite particles produced anaerobically by magnetotactic and dissimilatory iron-reducing bacteria *Geophys. Res. Lett.* **16** 665–8

[19] Moskowitz B M *et al* 1988 Magnetic properties of magnetotactic bacteria *J. Magn. Magn. Mater.* **73** 273–88

[20] Carvallo C *et al* 2009 Formation of magnetite in *Magnetospirillum gryphiswaldense* studied with FORC diagrams *Earth Planets Space* **61** 143–5

[21] Pan Y *et al* 2005 Rock magnetic properties of uncultured magnetotactic bacteria *Earth Planet. Sci. Lett.* **237** 311–25

[22] Charilaou M *et al* 2011 Evolution of magnetic anisotropy and thermal stability during nanocrystal-chain growth *Appl. Phys. Lett.* **99** 182504

[23] Prozorov R *et al* 2007 Magnetic irreversibility and the Verwey transition in nanocrystalline bacterial magnetite *Phys. Rev. B* **76** 054406

[24] Albrecht M *et al* 2005 Scanning force microspy study of biogenic nanoparticles for medical applications *J. Magn. Magn. Mater.* **290–291** 269–71

[25] Prozorov T *et al* 2013 Novel magnetic nanomaterials inspired by magnetotactic bacteria: topical review *Mater. Sci. Eng.* R **74** 133–72

[26] Lang C, Schüler D and Faivre D 2007 Synthesis of magnetite nanoparticles for bio- and nanotechnology: genetic engineering and biomimetics of bacterial magnetosomes *Macromol. Biosci.* **7** 144–51

[27] Proksch R B *et al* 1995 Magnetic force microscopy of the submicron magnetic assembly in a magnetotactic bacterium *Appl. Phys. Lett.* **66** 2582–4

[28] Wei J *et al* 2011 Magnetic properties of single biogenic magnetite nanoparticles *J. Nanopart. Res.* **13** 3345–52

[29] Wittborn J *et al* 1999 Magnetization reversal observation and manipulation of chains of nanoscale magnetic particles using the magnetic force microscope *Nanostruct. Mater.* **12** 1149–52

[30] Lang C, Pollithy A and Schuler D 2009 Identification of promoters for efficient gene expression in *Magnetospirillum gryphiswaldense Appl. Environ. Microbiol.* **75** 4206–10

[31] Hutter J L and Bechhoefer J 1993 Calibration of atomic-force microscope tips *Rev. Sci. Instrum.* **64** 1868–73

[32] Necas D and Klapetek P 2012 Gwyddion: an open-source software for SPM data analysis *Cent. Eur. J. Phys.* **10** 181–8

[33] Landau D P and Binder K 2009 *A Guide to Monte-Carlo Simulations in Statistical Physics* 3rd edn (Cambridge: Cambridge University Press)

[34] Grütter P, Rugar D and Mamin H J 1992 Magnetic force microscopy of magnetic-materials *Ultramicroscopy* **47** 393–9

[35] Babcock K *et al* 1995 Magnetic force microscopy: recent advances and applications *Evolution of Thin Film and Surface Structure and Morphology* vol 355 ed B G Demczyk *et al* pp 311–22

[36] Schleifer K-H *et al* 1991 The genus *Magnetospirillum* gen. nov., description of *Magnetospirillum gryphiswaldense* sp. nov. and transfer of *Aquaspirillum magnetotacticum* to *Magnetospirillum magnetotacticum* comb. nov. *Syst. Appl. Microbiol.* **14** 379–85

[37] Lang C and Schüler D 2008 Expression of green fluorescent protein fused to magnetosome proteins in microaerophilic magnetotactic bacteria *Appl. Environ. Microbiol.* **74** 4944–53

[38] Gorby Y A, Beveridge T J and Blakemore R P 1988 Characterization of the bacterial magnetosome membrane *J. Bacteriol.* **170** 834–41

[39] Dunlop D J and Özdemir O 1997 *Rock Magnetism: Fundamentals and Frontiers* Cambridge Studies in Magnetism (Cambridge: Cambridge University Press) p 596

[40] Häberle T *et al* 2012 Towards quantitative magnetic force microscopy: theory and experiment *New J. Phys.* **14** 043044

[41] Sievers S *et al* 2012 Quantitative measurement of the magnetic moment of individual magnetic nanoparticles by magnetic force microscopy *Small* **8** 2675–9